Dalton Transactions

PAPER

View Article Online
View Journal

Cite this: DOI: 10.1039/c7dt01957b

The role of KCl in $FeCl_3$–KCl/Al_2O_3 catalysts with enhanced catalytic performance for ethane oxychlorination†

Qihua Zhou, Ruisheng Hu, * Yun Jia and Hongye Wang

Received 30th May 2017,
Accepted 13th July 2017

DOI: 10.1039/c7dt01957b

rsc.li/dalton

Among the vinyl chloride production processes, ethane oxychlorination is the most economical and environment-friendly process but constrained by the lack of high performance catalysts for industrial applications. In this work, $FeCl_3$–KCl/Al_2O_3 catalysts with different molar ratios of K/Fe were prepared by a co-impregnation method and applied to ethane oxychlorination. The $FeCl_3$–KCl/Al_2O_3 catalyst with K/Fe = 2 exhibited enhanced catalytic performance with the highest conversion of C_2H_6 (99.1%) and the best selectivity to C_2H_3Cl (74%) under the optimal conditions of 400 °C, C_2H_6 : HCl : air = 1 : 3 : 5.5 (volume ratio) and GHSV = 4560 h^{-1}. It was found that the enhanced catalytic performance could be attributed to the formation of $KFeCl_4$ from KCl and $FeCl_3$ and the change of the reaction process. Besides, KCl is in favor of weakening the interaction between the active species and support. The reduction activation energy of Fe(III) → Fe(II) is efficiently reduced by KCl addition. The $FeCl_3$–KCl/Al_2O_3 catalyst may be a potential catalyst for industry due to its simple composition and convenient preparation.

1 Introduction

Poly-vinyl chloride (PVC) is one of the five general plastics and has been widely used in industry, agriculture, national defense and our daily life. The monomer of PVC, vinyl chloride, can be produced by three processes: acetylene hydrochlorination,[1–7] ethylene oxychlorination[8,9] and ethane oxychlorination.[10–14] The obvious drawback of acetylene hydrochlorination (based on the $HgCl_2/C$ catalyst) is high energy consumption and severe pollution. The cost of ethylene oxychlorination increases with the increase of the ethylene price. The most economical and environment-friendly process is ethane oxychlorination, which, however, is constrained by the lack of high performance catalysts for industrial applications. Therefore, the study of ethane oxychlorination is of great importance.

By far, the studies about the ethane oxychlorination catalyst have been focused on Cu-based catalysts. In 2006, Liu *et al.*[10] reported that the addition of KCl to the $CuCl_2/\gamma$-Al_2O_3 catalyst decreased the interaction between $CuCl_2$ and γ-Al_2O_3 and improved the catalytic performance by accelerating the Cu(II) → Cu(I) reduction. Xueju *et al.*[11] found that $CuCl_2$–KCl/γ-Al_2O_3 with $LaCl_3$ can achieve higher activity for ethane oxychlorination by making $CuCl_2$ highly dispersed and then preventing the catalyst from sintering. In 2011, a study by Li *et al.*[12] showed that the addition of CeO_2 to the catalyst could form aggregated crystalline ceria species and capping oxygen, which may enhance the performance of the catalyst. Meanwhile, in 2011, Li *et al.*[13] reported a binary promoter (La_2O_3, CeO_2) modified Cu-based catalyst for ethane oxychlorination, and found that the different impregnation procedures of the La_2O_3 precursor made a difference in catalytic activity. In 2013, Li *et al.*[14] assumed that Pr (Pr_6O_{11}) improved the electron transfer from Pr to Cu to promote the reduction of Cu species. In 2015, we reported that the addition of Cr species could effectively reduce the reduction activation energy of the Cu(II) → Cu(I) process in the $CuCl_2$–KCl–CeO_2/γ-Al_2O_3 catalyst.[15] Besides, we also reported a perovskite as a promoter for the Cu-based ethane oxychlorination catalyst.[16]These studies have deepened our knowledge about the Cu-based ethane oxychlorination catalyst and have made us realize its bottleneck of catalytic performance and its limited application in industrial production due to its complicated composition.

However, the current research about the Fe-based ethane oxychlorination catalyst is still rare. As we know, iron is one of the most abundant elements on earth, which is widely applied in the field of organic synthesis. Its kin element ruthenium has been widely applied in catalysis, especially in HCl oxidation (Deacon process).[17,18] The Deacon process plays a vital role in ethane oxychlorination. Considering the similarity

School of Chemistry and Chemical Engineering, Key Laboratory of Rare Earth Materials Chemistry and Physics, Inner Mongolia University, Hohhot 010021, P. R. China. E-mail: cehrs@imu.edu.cn

†Electronic supplementary information (ESI) available. See DOI: 10.1039/c7dt01957b

between iron and ruthenium, we shift the focus to the iron-based ethane oxychlorination catalyst. Goodrich Company developed a solid solution catalyst containing iron cations.[19] The catalyst contained iron cations of 1%–15% (weight percentage) and the yield of vinyl chloride reached 41.4% with iron cations of 4% (weight percentage). It is believed that it is important to continue the study about Fe-based ethane oxychlorination catalysts for the understanding of ethane oxychlorination and the improvement of the catalyst system. In this work, $FeCl_3$–KCl/Al_2O_3 catalysts with different molar ratios of K/Fe (denoted as FeKx, where x represents the molar ratio of K/Fe (x = 0, 0.5, 1, 1.5 and 2, respectively)) were prepared by a co-impregnation method and applied to ethane oxychlorination. The role of KCl in the $FeCl_3$–KCl/Al_2O_3 catalyst was studied by different characterization techniques. This work will deepen the comprehension about the active species in the $FeCl_3$–KCl/Al_2O_3 catalyst and of its role in ethane oxychlorination.

2 Experimental

2.1 Materials

All reagents ($FeCl_3{\cdot}6H_2O$, KCl) were analytical grade (≥99.0%) and obtained from Sinopharm Chemical Reagent Co., Ltd (Shanghai, China). Commercial γ-Al_2O_3 (≥99.7%) was obtained from ZiBo JuTeng Chemical Co., Ltd (Shandong, China). HCl (99.999%) and C_2H_6 (99.99%) were obtained from Dalian Special Gases Co., Ltd (Liaoning, China). HCl flow was controlled by using a mass flow controller. HCl was dried with a 5 A molecular sieve column before it passed the mass flow controller. C_2H_6 flow was treated under the same conditions just as HCl. Air was obtained with a SPB-3 air-source instrument (BCHP Analytical Technology Institute, Beijing, China).

2.2 Catalyst preparation

$FeCl_3$-KCl/Al_2O_3 catalysts with different molar ratios of K/Fe were prepared by the co-impregnation method. Commercial γ-Al_2O_3 (S_{BET} = 160.7 $m^2\ g^{-1}$) was chosen as the support. The support was mixed with an aqueous solution of appropriate $FeCl_3{\cdot}6H_2O$ (AR), KCl (AR), and impregnated by ultrasonication for 0.5 h, then aged for 24 h at room temperature and dried at 100 °C for 2 h. Later, the solid catalysts were calcined under an air atmosphere at 600 °C for 4 h. The catalysts with different molar ratios of K/Fe were denoted as FeKx, where x represents the molar ratio of K/Fe (x = 0, 0.5, 1, 1.5 and 2, respectively). All catalysts have the same content of iron, 5 wt% in γ-Al_2O_3.

2.3 Characterization

X-ray powder diffraction (XRD) patterns were recorded with an Empyrean X-ray diffractometer (PANalytical, Holland), using Cu Kα radiation, λ = 0.1542 nm, scanning step = 0.0065° s^{-1}, scanning over the range of 10° ≤ 2θ ≤ 80° and operating at 40 kV and 40 mA. The Brunauer–Emmett–Teller (BET) surface area was determined by nitrogen adsorption at 77 K on a Quantachrome Nova 4200e surface area and pore size analyzer. Before adsorption measurements, all samples were evacuated at 250 °C for 2 h. The total surface area was determined by the Brunauer–Emmett–Teller (BET) method. The pore volume was considered as the volume of liquid nitrogen adsorbed at $P/P_0 \approx 1$. H_2-TPR was conducted with a Chembet Pulsar multiple adsorption instrument (Quantachrome, USA). Before reduction, 0.1 g sample was loaded in a quartz tube reactor and pretreated in helium flow at 200 °C for 1 h to purge the sample surface. After cooling down to 50 °C, the reactor was heated from 50 °C to 900 °C at a heating rate of 10 °C min^{-1} in a 5% H_2/Ar gas flow of 35 ml min^{-1}. The consumption of hydrogen was monitored using a thermal conductivity detector (TCD). The ^{57}Fe Mossbauer spectra at room temperature were recorded by using an MFD-500A Mossbauer spectrometer (Topologic Systems, Japan). The radiation sources were ^{57}Co/Rh. The velocity was calibrated with α-Fe foil. The thickness of the absorbers used in the measurements is 3–5 mg Fe per cm^2. The spectra were fitted with the appropriate superpositions of Lorentzian lines using the MossWinn 3.0i computer program.

2.4 Catalytic tests

Catalytic activity of ethane oxychlorination was evaluated in a fixed bed quartz reactor (14 mm in internal diameter and 30 cm in length) under atmospheric pressure. Before reaction, the catalyst (1.0 g, 40–60 mesh) was activated under a HCl/air mixture (64 ml min^{-1}, HCl : air = 3 : 5) at 450 °C for 30 min. Then, ethane (8 ml min^{-1}) was dosed into the reactor. The reaction was carried out at 450 °C, C_2H_6 : HCl : air = 1 : 3 : 5, and total flow rate of 72 ml min^{-1}. The products were passed through a sodium hydroxide tank to remove hydrogen chloride. The reaction products were analyzed on an SP-6890 gas chromatograph (Lunan Ruihong Chemical Instrument Co. LTD, China) with a Porapak Q column and a TCD detector.

The conversion of ethane (X_A) and the selectivity to VCM (S_{VCM}) as the criteria of catalytic performance were calculated by equations: $X_A = (1 - \varphi_{air} - \varphi_A)/(1 - \varphi_{air}) \times 100\%$ and $S_{VCM} = \varphi_{VCM}/(1 - \varphi_{air} - \varphi_A) \times 100\%$ where φ_{air}, φ_A, and φ_{VCM} represent the volume fraction of air, the volume fraction of the remnant ethane, and the volume fraction of VCM, respectively.

We have conducted orthogonal experiments to study the effect of different ethane flow rates, different feed ratios and different reaction temperatures on the space–time yield of C_2H_3Cl. The studied factors and levels are listed in Table 1 and a $L_9(3^4)$ orthogonal table is used to design the orthogonal

Table 1 The studied factors and levels in orthogonal experiments

	Factor			
Level	Ethane flow rate (A)	The ratio of C_2H_6 to HCl (B)	The ratio of C_2H_6 to air (C)	Reaction temperature (D)
1	6 ml min^{-1}	1 : 1	1 : 5	400 °C
2	8 ml min^{-1}	1 : 2	1 : 5.5	450 °C
3	12 ml min^{-1}	1 : 3	1 : 6	470 °C

experiments. Other conditions in orthogonal experiments are the same as those stated above.

The Cl_2 release rate measurement was conducted under the same reaction conditions as stated above in a catalytic test but in the absence of ethane. 0.5 g catalyst (40–60 mesh) was loaded. When the reaction temperature reached 450 °C, the mixed gas of HCl (24 mL min^{-1}) and air (40 mL min^{-1}) was dosed into the reactor. After 30 min, KI solution (0.25 mol L^{-1}) was used to absorb the Cl_2 in the reaction products for 10 min. Iodometry was used to determine the amount of Cl_2 in the reaction products. 0.1 mol L^{-1} $Na_2S_2O_3$ solution was used in the titration.

3 Results and discussion

Fig. 1 shows the C_2H_6 conversion curves and the C_2H_3Cl selectivity curves of FeK*x* catalysts. As can be seen from Fig. 1a, the C_2H_6 conversion of potassium-containing samples (FeK*x*, x = 0.5, 1, 1.5, 2) is higher than that of the potassium-free sample (FeK0). In addition, the C_2H_6 conversion of FeK*x* catalysts increases with the increase of x in the following order: FeK0 < FeK0.5 < FeK1 < FeK1.5 < FeK2. As can be seen from Fig. 1b, the C_2H_3Cl selectivity curves of FeK*x* catalysts show a similar trend. The selectivity of potassium-containing samples (FeK*x*, x = 0.5, 1, 1.5, and 2) is higher than that of the potassium-free sample (FeK0). Besides, the C_2H_3Cl selectivity of FeK*x* catalysts also increases with the increase of x in the following order: FeK0 < FeK0.5 < FeK1 < FeK1.5 < FeK2. The FeK2 catalyst exhibits the highest C_2H_6 conversion (97.7%) and the best C_2H_3Cl selectivity (65.5%). The main by-product of the FeK2 catalyst is ethylene. The selectivity to ethylene is 34.3% and therefore the selectivity to other by-products like carbon dioxide is 0.2%. Besides, the loss of the active component is improved with the addition of KCl (Fig. S1 in ESI†).

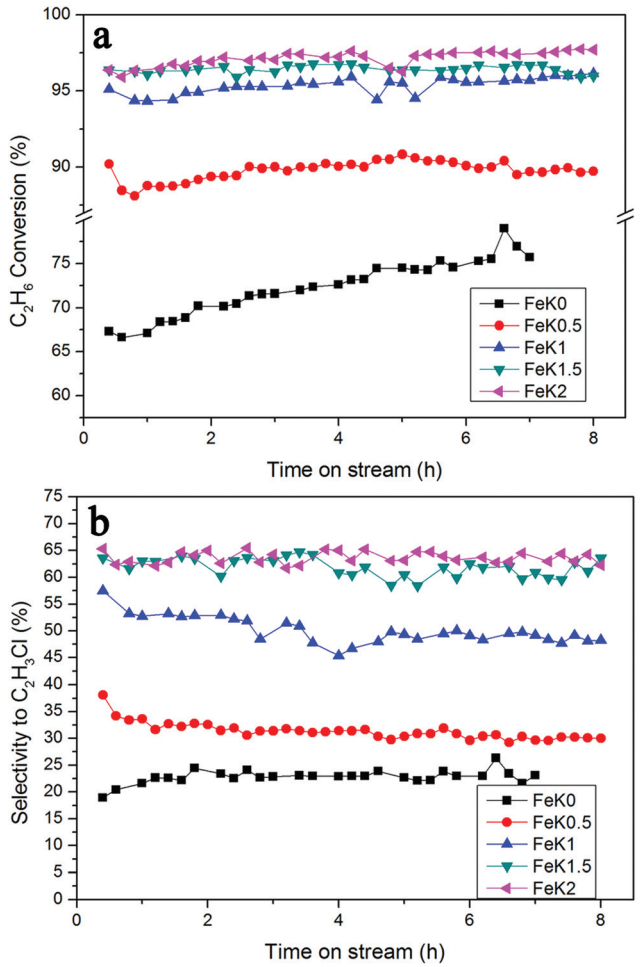

Fig. 1 The C_2H_6 conversion curves (a) and the C_2H_3Cl selectivity curves (b) of FeK*x* catalysts.

As can be seen in Fig. 1, the C_2H_6 conversion of the FeK0 catalyst increases in 7 h. Therefore, we performed a longer test on FeK0 (Fig. S2 in ESI†). It is found that the C_2H_6 conversion reaches its maximum (86.3%) after 12 h and enters a platform stage, while the C_2H_3Cl selectivity is quite stable. Compared with the potassium-containing catalysts, it suggests that the addition of KCl can shorten the time to enter the platform stage.

In industry, the catalytic performance is expressed by the space–time yield which includes the influence of the raw material flow rate. We also calculated the space–time yield (STY) of C_2H_3Cl using the following equation and the results are listed in Table 2:

$$\mathrm{STY} = \frac{m_p}{m_c \times T} = \frac{m_f \times \frac{M_p}{M_f} \times X_f \times S_p}{m_c \times T} = \frac{\frac{m_f}{M_f \times T} \times M_p \times X_f \times S_p}{m_c}$$

where $\frac{m_f}{M_f \times T}$ is the raw material (ethane) molar flow rate, M_p is the product (VCM) molar mass, X_f is the raw material conversion, S_p is the product selectivity, and m_c is the catalyst mass.

As can be seen from Table 2, the STY of FeK*x* catalysts increases with the increase of x, from 3.7 × 10^{-3} g g_{catal}^{-1} min^{-1} to 13.7 × 10^{-3} g g_{catal}^{-1} min^{-1}. The STY of FeK2 is about 3.7 times as large as that of FeK0. It is obvious that the addition of KCl is beneficial to the improvement of catalytic activity.

Table 2 The space–time yield (STY) of C_2H_3Cl of different catalysts

Catalyst	Average C_2H_6 conversion (%)	Average C_2H_3Cl selectivity (%)	STY (10^{-3} g g_{catal}^{-1} min^{-1})	Cl_2 release rate (10^{-5} mol min^{-1})
FeK0	72.5 ± 0.5	22.8 ± 0.2	3.7	7.17
FeK0.5	89.8 ± 0.1	31.4 ± 0.2	6.3	10.36
FeK1	95.4 ± 0.1	50.0 ± 0.4	10.6	15.76
FeK1.5	96.4 ± 0.1	61.9 ± 0.4	13.3	21.25
FeK2	97.1 ± 0.1	63.3 ± 0.3	13.7	22.34
KCl/Al_2O_3	59.7 ± 0.1	6.1 ± 0.1	0.8	

In order to prove the interaction between $FeCl_3$ and KCl, the catalytic performance of KCl/Al_2O_3 was also tested. The content of KCl in KCl/Al_2O_3 is equal to that of the FeK2 catalyst. KCl/Al_2O_3 exhibits poor catalytic activity (Fig. 2) with a C_2H_6 conversion of 60% and a C_2H_3Cl selectivity of 6%. The STY of FeK2 is larger than the sum STY of FeK0 and KCl/Al_2O_3, which suggests that the strong interaction between $FeCl_3$ and KCl such as a chemical reaction greatly improves the catalytic activity.

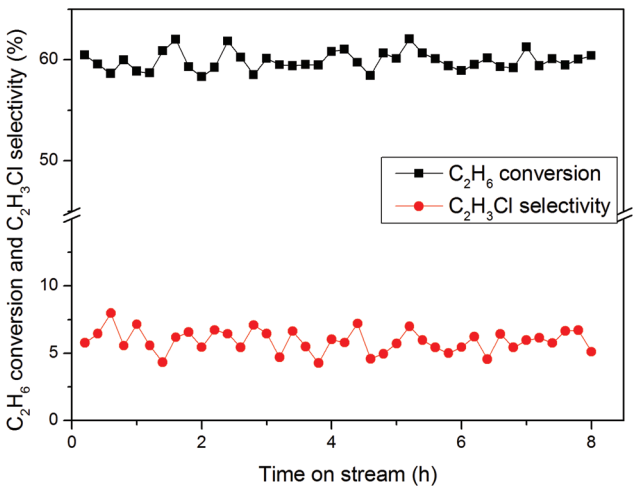

Fig. 2 The C_2H_6 conversion curve and the C_2H_3Cl selectivity curve of the KCl/Al_2O_3 catalyst.

We have conducted orthogonal experiments on the FeK2 catalyst in order to study the effect of different reaction conditions like raw material flow rate, feed ratio and reaction temperature on the C_2H_3Cl STY. The experimental results are shown in Table 3. Orthogonal analysis gives out the best reaction conditions of $A_3B_3C_2D_1$ which means that the FeK2 catalyst shows the highest STY with an ethane flow rate of 12 mL min^{-1}, the ratio of C_2H_6 to HCl of 1 : 3, the ratio of C_2H_6 to air of 1 : 5.5 and the reaction temperature of 400 °C. The range order of different factors is $B > A > D > C$. This indicates that the ratio of C_2H_6 to HCl and the ethane flow rate have a greater influence on the C_2H_3Cl STY. In our experiment, more HCl gives more Cl atoms in the reaction efficiently improving the ethane conversion. The larger the ethane flow rate is, the shorter the contact time between ethane and the catalyst becomes, avoiding the over-oxidation or over-chlorination of ethane and improving the product selectivity. Finally, we got a high C_2H_3Cl STY under the optimal conditions of 400 °C, C_2H_6 : HCl : air = 1 : 3 : 5.5 (volume ratio) and GHSV = 4560 h^{-1}.

As can be seen in Table 4, compared to the previous studies,[10–16] the FeK2 catalyst shows similar C_2H_6 conversion but obviously higher C_2H_3Cl selectivity with a lower reaction temperature (400 °C) and a larger ethane flow rate (12 mL min^{-1}).

Table 3 The orthogonal experiment results

	Reaction conditions				
Test number	Ethane flow rate (A)	The ratio of C_2H_6 to HCl (B)	The ratio of C_2H_6 to air (C)	Reaction temperature (D)	STY (10^{-3} g g_{catal}^{-1} min^{-1})
1	6 ml min^{-1}	1 : 1	1 : 5	400 °C	4.5
2	6 ml min^{-1}	1 : 2	1 : 5.5	450 °C	9.0
3	6 ml min^{-1}	1 : 3	1 : 6	470 °C	11.3
4	8 ml min^{-1}	1 : 1	1 : 5.5	470 °C	6.6
5	8 ml min^{-1}	1 : 2	1 : 6	400 °C	15.4
6	8 ml min^{-1}	1 : 3	1 : 5	450 °C	12.9
7	12 ml min^{-1}	1 : 1	1 : 6	450 °C	9.0
8	12 ml min^{-1}	1 : 2	1 : 5	470 °C	15.1
9	12 ml min^{-1}	1 : 3	1 : 5.5	400 °C	24.6

Table 4 Catalytic performance of different catalysts for ethane oxychlorination

	Conditions[a]					
Catalyst	Temperature	Feed ratio[b]	C_2H_6 conversion	C_2H_3Cl selectivity	C_2H_3Cl STY (10^{-3} g g_{catal}^{-1} min^{-1})	Ref.
$CuCl_2$–KCl/γ-Al_2O_3	500 °C	C_2H_6 : HCl : air = 1 : 3 : 5	89.9%	39.0%	3.9	10
$CuCl_2$–KCl-$LaCl_3$/γ-Al_2O_3	500 °C	C_2H_6 : HCl : air = 1 : 3 : 5	97.6%	51.7%	5.6	11
$CuCl_2$–KCl–CeO_2/MgO–γ-Al_2O_3	450–550 °C	C_2H_6 : HCl : air = 1 : 2 : 5	98.6%	55.2%	6.1	12
$CuCl_2$–KCl–CeO_2/La_2O_3/MgO–γ-Al_2O_3	450–550 °C	C_2H_6 : HCl : air = 1 : 2 : 5	97.0%	50.0%	5.4	13
$CuCl_2$–KCl–Pr_6O_{11}/MgO–γ-Al_2O_3	450–550 °C	C_2H_6 : HCl : air = 1 : 2 : 5	97.5%	52.0%	5.7	14
$CuCl_2$–KCl–CeO_2–Cr_2O_3/γ-Al_2O_3	510 °C	C_2H_6 : HCl : air = 1 : 3 : 5	97.8%	64.0%	14.0	15
$La_{1.7}K_{0.3}NiMnO_6$–$CuCl_2$/γ-Al_2O_3	500 °C	C_2H_6 : HCl : air = 1 : 3 : 5	100.0%	50.0%	11.2	16
$FeCl_3$–KCl/Al_2O_3	400 °C	C_2H_6 : HCl : air = 1 : 3 : 5.5	99.1%	74.0%	24.6	

[a] The reactor used is a fixed bed reactor. [b] The ethane flow rate is 4 mL min^{-1} for the catalysts in ref. 10–14, 8 mL min^{-1} for the catalysts in ref. 15 and 16 and 12 mL min^{-1} for the catalysts in this work.

Table 5 Specific surface area and reduction characteristics of FeKx catalysts

Catalyst	S_{BET} ($m^2\ g^{-1}$)	Theoretical H_2 consumption for Fe(III) to Fe(II) (mol)	Practical H_2 consumption (mol)	Reduction activation energy (kJ mol^{-1})
FeK0	154	4.06×10^{-5}	4.25×10^{-5}	55.93
FeK0.5	145	3.79×10^{-5}	3.89×10^{-5}	—
FeK1	132	3.70×10^{-5}	3.80×10^{-5}	—
FeK1.5	122	3.66×10^{-5}	3.84×10^{-5}	—
FeK2	113	3.53×10^{-5}	3.87×10^{-5}	47.37

The C_2H_3Cl STY of the FeK2 catalyst is much higher than that of the catalysts previously reported. Moreover, the FeK2 catalyst has a more simple composition, which is closer to the requirement of industrial application.

N_2 adsorption/desorption experiments were carried out to study the textural properties of FeK*x* catalysts. As can be seen from Fig. S3,† the shape of the N_2-adsorption/desorption isotherms does not change obviously, suggesting that the loading of active species does not change the pore structure in the support. Besides, the BET surface area decreases with the increase of K/Fe (Table 5). The BET surface area reduces by 26.6% (from 154 $m^2\ g^{-1}$ to 113 $m^2\ g^{-1}$) because of the loading of the active species.

XRD was conducted to figure out the phase composition of the catalysts (Fig. 3). The characteristic peaks of γ-Al_2O_3 are observed in the XRD patterns of all catalysts. When the K/Fe is larger than 1, the diffraction peaks of KCl (2θ = 28.36, 40.53, 66.42°) strengthen gradually. In the case of FeK0, the characteristic peaks of $FeCl_3$ cannot be observed in its XRD pattern. Zong and Xie *et al.*[20] reported that $FeCl_3$ could disperse spontaneously onto the γ-Al_2O_3 surface. The dispersion threshold of $FeCl_3$ is 2.1 mg m^{-2}, which means that the amount of $FeCl_3$ to form a monolayer on our γ-Al_2O_3 (S_{BET} = 160.7 $m^2\ g^{-1}$) is 0.3375 g g^{-1}, more than the amount of $FeCl_3$ (0.1453 g g^{-1}) in our samples. It is assumed that the content of $FeCl_3$ is lower than its dispersion threshold so $FeCl_3$ is highly dispersed on the support. In the potassium-containing catalysts (FeK*x*, *x* = 0.5, 1, 1.5, 2), there are no diffraction peaks of $FeCl_3$ or other iron species, indicating that the iron species are also highly dispersed.

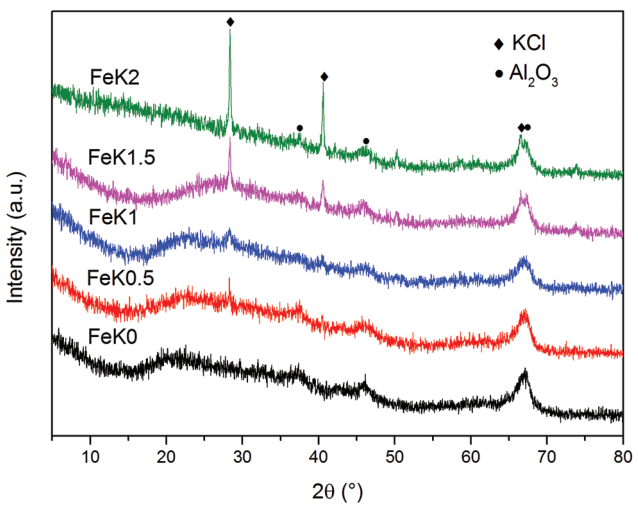

Fig. 3 The XRD patterns of FeK*x* catalysts.

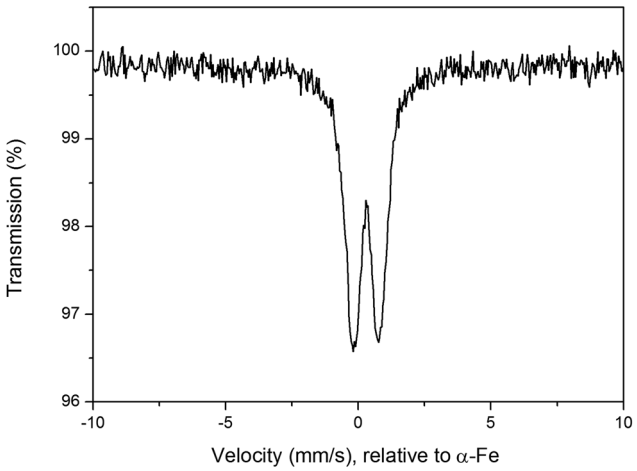

Fig. 4 The Mossbauer spectrum of the FeK2 catalyst.

Mossbauer spectroscopy can be applied to qualitative and quantitative analysis for complicated materials by comparing the Mossbauer parameters such as isomer shift (I.S.) and quadrupole splitting (Q.S.).[21] The iron content in our catalysts is relatively low and the iron species is highly dispersed, which is proved by XRD results. Therefore, the Mossbauer spectrum of FeK2 is studied. The I.S. of pure $FeCl_3$ is 0.45 mm s^{-1}.[22] The I.S. of pure $KFeCl_4$ is 0.29 mm s^{-1}.[22] According to the Mossbauer spectrum (Fig. 4), the FeK2 catalyst shows a doublet with an I.S. of 0.301 mm s^{-1} and Q.S. of 1.346 mm s^{-1}. The I.S. of the FeK2 catalyst is in accordance with that of $KFeCl_4$ but the Q.S. is much higher than that of $KFeCl_4$. Considering the composition of the FeK2 catalyst, we interpret these as that iron exists in the form of $KFeCl_4$. However, because the iron species highly disperse on the support as a monolayer, the $KFeCl_4$ on the support has lower structure symmetry which leads to a high Q.S. value. It is the high sensitivity and energy resolution of the Mossbauer spectrum[23] that makes the observation of the existence of $KFeCl_4$ on the catalyst possible.

H_2-TPR is a very effective technique for studying the reduction behavior of the catalyst. Fig. 5 shows the H_2-TPR profiles of FeK*x* catalysts. As we see, each catalyst shows a complete peak around 500 °C–550 °C which is mainly discussed below. The peak around 500 °C–550 °C is attributed to the reduction process of Fe(III) → Fe(II) by comparing the practical H_2 consumption with the theoretical H_2 consumption for Fe(III) → Fe(II) (Table 5). The potassium-free sample (FeK0) shows a broad peak with lower intensity, suggesting a strong interaction between the active species and support. However, potassium-containing samples (FeK*x*, *x* = 0.5, 1, 1.5, 2) show

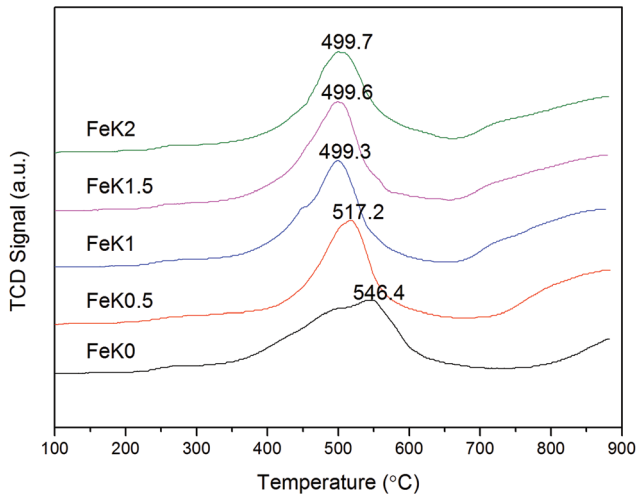

Fig. 5 The H_2-TPR profiles of FeK*x* catalysts.

narrow peaks with higher intensity, which means that KCl can weaken the interaction between the active species and support.[10] In addition, the reduction temperature of Fe(III) → Fe(II) decreases and then stabilizes at about 500 °C with the increase of K/Fe. When $x = 0$, it is $FeCl_3$ that is reduced by H_2. When $x = 0.5$, $FeCl_3$ is excessive and part of $FeCl_3$ forms $KFeCl_4$ with KCl. When $x \geq 1$, all $FeCl_3$ forms $KFeCl_4$ with excessive KCl theoretically.[24–27] Therefore, the reduction temperature of Fe(III) → Fe(II) stabilizes at about 500 °C (the maximal temperature difference (0.4 °C) is less than the experimental error). The decrease of reduction temperature suggests the change of active species ($FeCl_3$ → $KFeCl_4$).

In order to study the effect of the addition of KCl on the reduction activation energy of Fe(III) → Fe(II), the reduction activation energy of Fe(III) → Fe(II) of FeK0 and FeK2 catalysts is calculated. Fig. S4† shows the H_2-TPR curves of FeK0 and FeK2 at different heating rates (β). It is observed that the reduction peaks of Fe(III) → Fe(II) of FeK0 and FeK2 moved to higher temperature with the increasing heating rate (β), also with the increase of peak intensity.

As shown in Table 5 and Fig. S5,† the reduction activation energy of reduction of Fe(III) → Fe(II) of FeK0 and FeK2 is 55.93 kJ mol^{-1} and 47.37 kJ mol^{-1}, respectively. Comparing the reduction activation energy of FeK0 and FeK2, the reduction activation energy of FeK2 is obviously lower than FeK0, which indicates that the addition of KCl is responsible for the easier activation and reduction of Fe(III).

In a Cu-based catalyst, the release of Cl_2 is the key of the whole oxychlorination process.[12,28] Ethane conversion and vinyl chloride selectivity can be improved by accelerating the release of Cl_2.[10,15] This is also true for our FeK*x* catalysts. In order to compare the Cl_2 release efficiency, we have measured the Cl_2 release rate of FeK*x* catalysts and the results are listed in Table 2. It can be seen that the Cl_2 release rate increases in the following order: FeK0 < FeK0.5 < FeK1 < FeK1.5 < FeK2. This is in accordance with the order of C_2H_3Cl STY of FeK*x* catalysts. It is interesting that the Cl_2 release rate of FeK2 is about 3 times as fast as that of FeK0, while the C_2H_3Cl STY of FeK2 is about 3.7 times as large as that of FeK0. It suggests that the C_2H_3Cl STY is strongly related to the Cl_2 release efficiency. The addition of KCl to $FeCl_3/Al_2O_3$ changes the active species from $FeCl_3$ to $KFeCl_4$, and also the Cl_2 release efficiency. $KFeCl_4$, reacting with O_2, releases Cl_2 with higher efficiency (eqn (1)). $KFeO_2$, reacting with HCl, generates $KFeCl_4$ to form a cycle (eqn (2)). More Cl_2 is favorable to the transformation of ethane to vinyl chloride.[28] These are important for $FeCl_3$–KCl/Al_2O_3 being an ethane oxychlorination catalyst with enhanced catalytic performance and explain why the catalytic performance of potassium-containing samples (FeK*x*, $x = 0.5, 1, 1.5, 2$) is better than that of the potassium-free sample (FeK0).

$$KFeCl_4 + O_2 \rightarrow KFeO_2 + 2Cl_2 \quad (1)$$

$$KFeO_2 + 4HCl \rightarrow KFeCl_4 + 2H_2O \quad (2)$$

4 Conclusion

Generally, $FeCl_3$–KCl/Al_2O_3 catalysts were prepared by the co-impregnation method and applied to ethane oxychlorination. It is observed that the C_2H_6 conversion and the C_2H_3Cl selectivity of FeK*x* catalysts increase with the increase of *x* in the following order: FeK0 < FeK0.5 < FeK1 < FeK1.5 < FeK2. The FeK2 catalyst exhibits the highest C_2H_6 conversion (99.1%) and the best C_2H_3Cl selectivity (74%) under the optimal conditions of 400 °C, C_2H_6 : HCl : air = 1 : 3 : 5.5 (volume ratio) and GHSV = 4560 h^{-1}. It is found that the enhanced catalytic performance can be attributed to the formation of $KFeCl_4$ from KCl and $FeCl_3$. The addition of KCl can reduce the reduction activation energy of Fe(III) → Fe(II). Besides, KCl is in favor of weakening the interaction between the active species and support which is good for the proceeding of ethane oxychlorination.

Conflict of interest

There is no conflict of interest to declare.

Acknowledgements

This work was financially supported by the National Natural Science Foundation of China (No. 21566027). The authors would like to appreciate the support from Inner Mongolia Autonomous Region Open Funding for Major Basic Research of China.

References

1 G. J. Hutchings, Nanocrystalline gold and gold palladium alloy catalysts for chemical synthesis, *Chem. Commun.*, 2008, 1148–1164.

2 H. Y. Zhang, B. Dai, X. G. Wang, W. Li, Y. Han, J. J. Gu and J. L. Zhang, Non-mercury catalytic acetylene hydrochlorination over bimetallic Au–Co(III)/SAC catalysts for vinyl chloride monomer production, *Green Chem.*, 2013, **15**, 829–836.
3 M. Conte, C. J. Davies, D. J. Morgan, T. E. Davies, D. J. Elias, A. F. Carley, P. Johnston and G. J. Hutchings, Aqua regia activated Au/C catalysts for the hydrochlorination of acetylene, *J. Catal.*, 2013, **297**, 128–136.
4 M. Conte, A. F. Carley, C. Heirene, D. J. Willock, P. Johnston, A. A. Herzing, C. J. Kiely and G. J. Hutchings, Hydrochlorination of acetylene using a supported gold catalyst: A study of the reaction mechanism, *J. Catal.*, 2007, **250**, 231–239.
5 M. Conte, A. F. Carley, G. Attard, A. A. Herzing, C. J. Kiely and G. J. Hutchings, Hydrochlorination of acetylene using supported bimetallic Au-based catalysts, *J. Catal.*, 2008, **257**, 190–198.
6 B. Nkosi, M. D. Adams, N. J. Coville and G. J. Hutchings, Hydrochlorination of acetylene using carbon-supported gold catalysts: A study of catalyst reactivation, *J. Catal.*, 1991, **128**, 378–386.
7 B. Nkosi, N. J. Coville, G. J. Hutchings, M. D. Adams, J. Friedl and F. E. Wagner, Hydrochlorination of acetylene using gold catalysts: A study of catalyst deactivation, *J. Catal.*, 1991, **128**, 366–377.
8 E. Finocchio, N. Rossi, G. Busca, M. Padovan, G. Leofanti, B. Cremaschi, A. Marsella and D. Carmello, Characterization and catalytic activity of $CuCl_2$-Al_2O_3 ethylene oxychlorination catalysts, *J. Catal.*, 1998, **179**, 606–618.
9 N. B. Muddada, U. Olsbye, T. Fuglerud, S. Vidotto, A. Marsella, S. Bordiga, D. Gianolio, G. Leofanti and C. Lamberti, The role of chlorine and additives on the density and strength of Lewis and Brønsted acidic sites of γ-Al_2O_3 support used in oxychlorination catalysis: A FTIR study, *J. Catal.*, 2011, **284**, 236–246.
10 J. Liu, X. J. Lǔ, G. D. Zhou, K. J. Zhen, W. X. Zhang and T. X. Cheng, Effect of KCl on $CuCl_2$/γ-Al_2O_3 catalyst for oxychlorination of ethane, *React. Kinet. Catal. Lett.*, 2006, **88**, 315–323.
11 L. Xueju, L. Jie, Z. Guangdong, Z. Kaiji, L. Wenxing and C. Tiexin, Ethane oxychlorination over γ-Al_2O_3 supported $CuCl_2$–KCl–$LaCl_3$, *Catal. Lett.*, 2005, **100**, 153–159.
12 C. Li, G. D. Zhou, L. P. Wang, S. L. Dong, J. Li and T. X. Cheng, Effect of ceria on the MgO-γ-Al_2O_3 supported CeO_2/$CuCl_2$/KCl catalysts for ethane oxychlorination, *Appl. Catal., A*, 2011, **400**, 104–110.
13 C. Li, G. D. Zhou, L. P. Wang, Z. Li, Y. X. Xue and T. X. Cheng, Effect of impregnation procedure of La_2O_3 precursor on copper-based catalysts for ethane oxychlorination, *Catal. Commun.*, 2011, **13**, 22–25.
14 Z. Li, G. D. Zhou, C. Li and T. X. Cheng, Effect of Pr on copper-based catalysts for ethane oxychlorination, *Catal. Commun.*, 2013, **40**, 42–46.
15 D. Z. Shi, R. S. Hu, Q. H. Zhou and C. Li, Effect of Cr-doping on $CuCl_2$-KCl-CeO_2/γ-Al_2O_3 catalysts for ethane oxychlorination, *Appl. Catal., A*, 2015, **506**, 91–99.
16 D. Z. Shi, R. S. Hu, Q. H. Zhou and L. R. Yang, Catalytic activities of supported perovskite promoter catalysts La_2NiMnO_6–$CuCl_2$/γ-Al_2O_3 and $La_{1.7}K_{0.3}NiMnO_6$–$CuCl_2$/γ-Al_2O_3 for ethane oxychlorination, *Chem. Eng. J.*, 2016, **288**, 588–595.
17 D. Crihan, M. Knapp, S. Zweidinger, E. Lundgren, C. J. Weststrate, J. N. Andersen, A. P. Seitsonen and H. Over, Stable Deacon Process for HCl oxidation over RuO_2, *Angew. Chem., Int. Ed.*, 2008, **120**, 2161–2164.
18 H. Over, Atomic-scale understanding of the HCl oxidation over RuO_2, a novel Deacon Process, *J. Phys. Chem. C*, 2012, **116**, 6779–6792.
19 W. J. Kroenke and P. P. Nicholas, Process for the oxychlorination of an alkane using a solid solution catalyst containing iron cations, *US patent*, 4375569, 1983.
20 Y. Zong, X. M. Pan, L. Y. Duan and Y. C. Xie, Dispersion state and dispersion capacity of $AlCl_3$ and $FeCl_3$ on γ-Al_2O_3 surface, *Chin. J. Catal.*, 1997, **18**, 321–323.
21 J. M. Millet, Mossbauer spectroscopy in heterogeneous catalysis, *Adv. Catal.*, 2007, **51**, 309–350.
22 Y. Takashima, Y. Maeda and S. Umemoto, The Mossbauer spectrum of iron adsorbed on an anion exchange resin, *Bull. Chem. Soc. Jpn.*, 1969, **42**, 1760–1761.
23 K. Liu, A. I. Rykov, J. H. Wang and T. Zhang, Recent advances in the application of Mossbauer spectroscopy in heterogeneous catalysis, *Adv. Catal.*, 2015, **58**, 1–142.
24 H. L. Friedman, The visible and ultraviolet absorption spectrum of the tetrachloroferrate(III) ion in various media, *J. Am. Chem. Soc.*, 1952, **74**, 5–10.
25 C. M. Cook and W. E. Dunn, The reaction of ferric chloride with sodium and potassium chlorides, *J. Phys. Chem.*, 1961, **65**, 1505–1511.
26 P. Palvadeau, J. Cerisier, C. Guiilot, J. P. Venien, E. Rzepka and S. Lefrant, Vibrational spectra and force constants of the alkali tetrahalogenoferrates $MFeCl_4$ (M=Li, Na, K, Rb, Cs), *Solid State Commun.*, 1990, **75**, 383–387.
27 M. Prien and H. J. Seifert, Thermochemical and structural investigations on alkali metal chlorides-iron(III)-chloride systems, *J. Therm. Anal.*, 1995, **45**, 349–358.
28 I. M. Dahl, E. M. Myhrvold, U. Olsbye, F. Rohr, O. A. Rokstad and O. Swang, On the gas-phase chlorination of ethane, *Ind. Eng. Chem. Res.*, 2001, **40**, 2226–2235.